Bulletin of Earthquake Engineering
https://doi.org/10.1007/s10518-021-01129-6

ORIGINAL ARTICLE

A discrete-cracking numerical model for the in-plane behavior of FRCM strengthened masonry panels

Francesco Saverio Murgo[1] · **Francesca Ferretti**[1] · **Claudio Mazzotti**[1]

Received: 17 July 2020 / Accepted: 16 May 2021

Abstract
In this paper, the structural behavior of masonry panels strengthened with a system made up of composite fiber grids embedded in a cementitious matrix (FRCM) is presented. The non-linear behavior of the unreinforced and reinforced panels is numerically simulated by means of a simplified micro-modelling approach. This approach concentrates all the non-linearities and failures in the joints and in potential crack surfaces within the bricks, placed vertically in the middle of each brick. The FRCM strengthening system is discretized by a continuous bi-directional fiber grid constituted by trusses embedded into a cementitious matrix. A calibrated bond-slip relationship is applied between the fibers and the mortar matrix assuming an idealized bilinear law. The typical experimental load–displacement curve for a FRCM strengthened panel shows three principal phases that correspond to different failure mechanisms: masonry cracking, mortar matrix cracking and ultimate failure of the panel. The non-linear numerical analyses show a good agreement with experimental results and the modeling approach is found to be adequate to reproduce the described experimental behavior. The results of a parametric study on both the material and the geometrical properties of the FRCM system are also presented.

Keywords Masonry · Fiber reinforced cementitious matrix · Diagonal compression tests · FEM · Numerical modeling

1 Introduction

The damages caused by the most severe earthquakes in recent decades, some of which catastrophic, have drawn attention to the problem of the vulnerability of the historical architectural heritage, consisting mostly of masonry buildings (Penna et al. 2014; Penna

✉ Francesca Ferretti
francesca.ferretti10@unibo.it

Francesco Saverio Murgo
francesco.murgo2@unibo.it

Claudio Mazzotti
claudio.mazzotti@unibo.it

[1] Department of Civil, Chemical, Environmental and Materials Engineering, University of Bologna, Viale Risorgimento 2, 40136 Bologna, Italy

Published online: 28 May 2021

2015; Ferretti et al. 2019a). For this reason, the interest in the strengthening of masonry structures has significantly grown especially concerning techniques that allow to perform reversible, compatible and sustainable interventions, guaranteeing an adequate level of safety for the buildings against vertical loads and even more against forces acting in a horizontal direction.

In this framework, the use of fiber reinforced polymers (FRP) to strengthen masonry panels became very popular due to the extremely low weight-to-strength ratio, the ease of application, and the capability of maintaining the original stiffness of the unstrengthened element. These materials, characterized by the presence of an organic matrix, within which fibers are embedded, present some critical aspects, such as the poor compatibility with the masonry substrate and a limited fire resistance. Recently, to overcome the highlighted issues, an alternative to FRP emerged for the strengthening of masonry structures, consisting of fibers embedded in an inorganic mortar matrix (Fiber Reinforced Cementitious Matrix—FRCM).

There are several experimental studies about the effectiveness of FRCM reinforcements applied to masonry walls (Prota et al. 2006; Faella et al. 2010; Balsamo et al. 2011; Parisi et al. 2013; Balsamo and Iovinella 2014; Corradi et al. 2014; Babaeidarabad et al. 2014; Gattesco et al. 2015; Gattesco and Boem 2015; Menna et al. 2015; Mustafaraj and Yardim 2016; Yardim and Lalaj 2016; Mininno et al. 2017; de Carvalho Bello et al. 2017; Lignola et al. 2017; de Felice et al. 2018; Giaretton et al. 2018; Incerti et al. 2019a, b; Bellini et al. 2019b; Del Zoppo et al. 2019a; Ferretti et al. 2019b; De Santis et al. 2019; Türkmen et al. 2020). As a general outcome, the FRCM reinforcements appeared to be very effective in improving the shear behavior of the masonry walls, both in terms of ultimate load and failure mode.

There are several numerical studies about the effectiveness of FRP systems applied to masonry (Verhoef and van Zijl 2002; van Zijl and de Vries 2005; Gabor et al. 2005, 2006; Ascione et al. 2005; Grande et al. 2008; Petersen et al. 2010, 2012; Ceroni et al. 2014; Mazzotti and Murgo 2015); on the contrary, very few recent works investigated the behavior of masonry structures strengthened by FRCM systems (Garofano et al. 2016; Basili et al. 2016; Wang et al. 2016, 2017; Bertolesi et al. 2016; Murgo and Mazzotti 2017, 2019; Bellini et al. 2019a). The numerical modelling of FRCM strengthened elements is quite complex, adding to the specific aspects of the masonry (Giamundo et al. 2014; Sarhosis and Lemos 2018) further issues related to the composite system, its bond to the substrate and the possible internal fiber-to-mortar matrix delamination.

The aim of this paper is the numerical investigation of the in-plane behavior of FRCM strengthened masonry panels following the *simplified micro-modelling* approach developed by Lourenço and Rots (Lourenço 1996; Rots 1997; Lourenço and Rots 1997), also known in literature as *meso-scale* approach (Macorini and Izzuddin 2011; Aref and Dolatshahi 2013). The main objective, within the framework of the cited numerical approach, is to specifically model each single FRCM component: mortar matrix, fibers and their interface.

In literature (Garofano et al. 2016; Basili et al. 2016; Wang et al. 2017), the modelling and analysis of FRCM systems are performed by using a macro-modelling approach based on a smeared crack theory for masonry, with the assumption of having a layer of external mortar homogenized with distributed reinforcement, fully embedded inside the matrix elements. Correspondingly, the displacements and the strains of the FRCM system are fully coupled with the masonry substrate through the hypothesis of a perfect bond between the two components. Some research works analyze the debonding of the FRCM system from the substrate (Carozzi et al. 2014; Bertolesi et al. 2014) proposing a simplified analytical–numerical approach to model the interaction of the grids with the mortar matrix, and

a sophisticated 3D model, where the interface behavior between mortar matrix and grid is based on the stress-slip curves deduced from experimental data.

An improved *simplified micro-modelling* approach is proposed in this paper to include the presence of the FRCM strengthening system. More in detail, the approach consists of modelling the masonry trough a discrete cracking approach and then introducing individually each fiber bundle embedded in the mortar matrix trough a bond-slip law. The mortar matrix, as the masonry, can present discrete cracks and it is perfectly bonded to the substrate. The quality and refinement of the adopted mesh is the result of a balance between the obtainable results and the relative computational effort, especially for the modeling of the FRCM strengthened panel. Moreover, the choice about the mesh refinement is the result of a mesh sensitivity analysis, in which two different meshes are compared: a rough one and a very detailed one; in the first case, the results would not be satisfactory, while in the second, instead, the model requires a significant computational effort. For these reasons, an intermediate mesh refinement is chosen, as will be explained in the following.

A 2D numerical description of the problem is considered, by using the commercial code DIANA FEA 10.1, and numerical outcomes are compared with experimental ones (Ferretti et al. 2016, 2017) in order to validate the proposed approach and understand the capabilities and limitations of the model. In particular, the 2D modelling is chosen since the masonry panels, in the considered experimental campaigns, were single-leaf walls, with a regular bond pattern. The numerical analyses are performed by modelling one specific carbon FRCM system, whose bond-slip law is calibrated on the basis of experimental bond tests. Finally, a parametric analysis is developed on the FRCM strengthened panel model to investigate the influence of each parameter on the non-linear response. More in detail, variations in the mechanical properties of the mortar matrix, in the bond-slip relation between fibers and mortar matrix, and in the amount of reinforcing fibers are investigated.

2 Masonry model

In order to describe and analyze the mechanical behavior of masonry panels strengthened by FRCM, the first step is to introduce a reliable and validated model for the unreinforced masonry, able to describe the distinct directional properties exhibited by masonry due to the mortar joints (Fig. 1a), which act as planes of weakness. Numerical models depend on the desired level of accuracy, simplicity and size. Correspondingly, different modelling

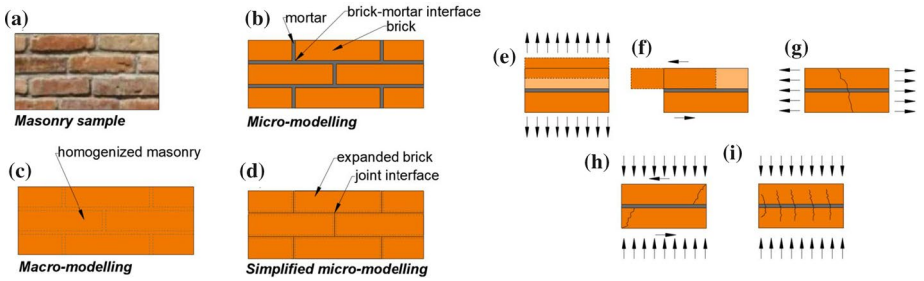

Fig. 1 Masonry model and masonry failure mechanisms: **a** masonry sample, **b** detailed micro-modelling, **c** macro-modelling, **d** simplified micro-modelling, **e** joint tensile cracking, **f** joint slipping, **g** unit direct tensile cracking, **h** unit diagonal tensile cracking, **i** masonry crushing

strategies can be used, belonging to the following rough categories: micro-modelling and macro-modelling approaches.

According to the micro-modelling approach (Fig. 1b), the individual components of the masonry assemblage are modelled separately: clay bricks and mortar are represented by continuum elements and brick–mortar interfaces are represented by discontinuous elements. In the macro-modelling approach (Fig. 1c), instead, bricks, mortar and brick–mortar interfaces are smeared out in the continuum. In this case, description of discontinuous failure modes (cracks) can be done only in an approximate way, but the computational effort is reduced and the modelling of large section of masonry can be done efficiently.

Within the first category, it is possible to use a different strategy, that represents a compromise between the two approaches and it is called *simplified micro-modelling* (Fig. 1d) (Wang et al. 2016), in which the bricks, expanded to maintain the overall geometry unchanged, are represented by continuum elements, while the behavior of the mortar joints and of the brick–mortar interfaces is lumped in a zero-thickness interface. In this paper, the simplified micro-modelling approach described by Lourenço (Lourenço 1996; Lourenço and Rots 1997) is adopted to model the masonry behavior; in particular, a two-dimensional finite element mesh and corresponding numerical model are adopted to simulate the non-linear behavior of the masonry panels. The commercial FE software DIANA FEA 10.1 is used for this study.

According to the chosen modelling approach, each joint, consisting of mortar and two brick–mortar interfaces, is lumped into an average interface element while the bricks, modelled with continuum elements, are expanded to keep the geometry unchanged. Interface elements are also used at mid-length of each brick to model potential cracking through the middle of the bricks; the bricks are considered made of a linear elastic material and all the non-linearities of the problem are lumped in the interface elements. Figure 2 shows a simplified description of the adopted masonry model, in which all interfaces were drawn with a given thickness for reason of clarity. Further details about interface modelling in masonry, including parameter determination and practical examples, can be found in (Rots 1997; Lourenço and Rots 1997).

The non-linear behavior in the mortar joint interface elements is modelled using the combined cracking-shearing-crushing material model included in DIANA FEA, developed by Lourenço and Rots (Lourenço 1996; Lourenço and Rots 1997) and improved by Van Zijl (2004). This model includes all the basic types of failure mechanism that characterize masonry (Fig. 1e–i): cracking of the joints, sliding along bed or head joints at low values of normal stress, cracking of the bricks in direct tension, brick diagonal tensile cracking and masonry crushing. The introduced interface material model, also known as the *Composite Interface model*, is appropriate to simulate fracture, frictional

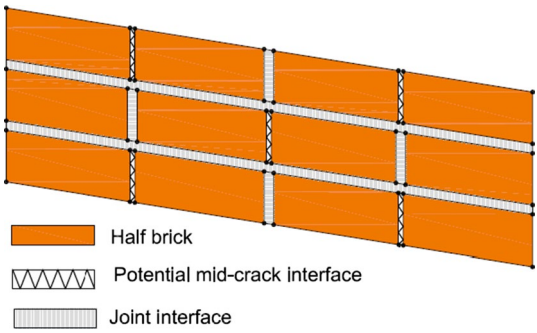

Fig. 2 Simplified micro-modelling approach

slip as well as crushing along material interfaces, for instance at joints in masonry. Cap models, originated in the field of soil mechanics, were firstly made for the purpose of describing plastic compaction and to enhance the behavior under hydrostatic compression (Drucker et al. 1957).

The adopted plane interface model is based on multi-surface plasticity, comprising a Coulomb friction model $f_1(\sigma, \kappa_1)$ combined with a tension cut-off $f_2(\sigma, \kappa_2)$ and an elliptical compression cap $f_3(\sigma, \kappa_3)$. In Fig. 3, the composite interface model (Fig. 3a) is reported together with the constitutive models for the different failure modes (Fig. 3b-e), which are expressed as stress (τ or σ) versus interface relative displacements (tangential displacement Δv or normal displacement Δu) or plastic strain (κ).

For the Coulomb friction mode, the yield function reads:

$$f_1(\sigma, \kappa_1) = |\tau| + \sigma \tan \phi(\kappa_1) - \overline{\sigma}_1(\kappa_1), \tag{1}$$

where the yield value $\overline{\sigma}_1$ can be expressed as:

$$\overline{\sigma}_1(\kappa_1) = c e^{-\frac{c}{G_f^{II}} \kappa_1}, \tag{2}$$

and the friction angle ϕ is coupled with cohesion softening via the expression:

$$\tan \phi = \tan \phi_0 + (\tan \phi_r - \tan \phi_0) \frac{c - \overline{\sigma}_1(\kappa_1)}{c}, \tag{3}$$

where c is the cohesion of the brick–mortar interface, ϕ_0 and ϕ_r are the initial and the residual friction angles, respectively, G_f^{II} is the mode-II fracture energy and κ_1 is an internal softening parameter that controls the softening behavior (Fig. 3b). Exponential softening is assumed for the cohesion, and, for simplicity, the softening of the friction angle is taken proportional to the cohesion softening. This last assumption leads to non-constant mode-II fracture energy under increasing confining pressure.

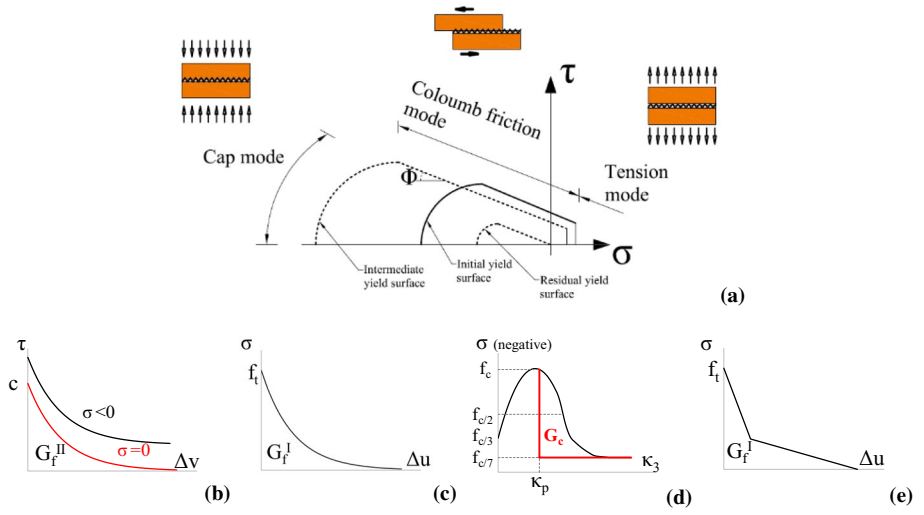

Fig. 3 Constitutive models: **a** failure surface of the cracking-shearing-crushing model, **b** shear mode, **c** tension mode, **d** compression mode, **e** tension-softening model for the potential crack in the bricks

For the tension mode, exponential softening on the tensile strength is assumed according to the mode-I experiments (Van der Pluijm 1997). The corresponding yield function reads:

$$f_2(\sigma, \kappa_2) = \sigma - \overline{\sigma}_2(\kappa_2), \tag{4}$$

with:

$$\overline{\sigma}_2(\kappa_2) = f_t e^{-\frac{f_t}{G_f^I}\kappa_2}, \tag{5}$$

where f_t is the tensile strength of the joint or, more precisely, of the brick–mortar interface, which generally is the weakest link, and G_f^I is the mode-I fracture energy (Fig. 3c).

For the cap model, the ellipsoid interface model firstly introduced by Schellekens (Schellekens 1992) for orthotropic plasticity in a 3D configuration is used. The yield function, for a 2D configuration, is given by:

$$f_3(\sigma, \kappa_3) = C_{mm}\sigma^2 + C_{ss}\tau_2 + C_n\sigma - (\overline{\sigma}_3(\kappa_3))^2, \tag{6}$$

where C_{mm}, $C_{ss,}$ and C_n are a set of material parameters and $\overline{\sigma}_3$ is the yield value.

The parameters C_{mm} and C_n control the center of the cap and its intersection with the tensile part of the normal stress axis whereas the parameter C_{ss} controls the contribution of the shear stress to failure. The cap mode is described by a parabolic hardening rule, until the peak compressive strength of the masonry is reached at the plastic strain κ_p (Fig. 3d). The value of the plastic deformation at peak was calculated trough the expression:

$$\kappa_p = f_c\left(\varepsilon_t - f_c\left(\frac{1}{E_u} + \frac{1}{k_n(h_u + h_m)}\right)\right), \tag{7}$$

where h_u e h_m are the brick and mortar joint heights, respectively, ε_t is the masonry total deformation at peak, f_c is the compressive strength of the brick-joint system, which can be determined as (Atkinson and Noland 1983):

$$f_c = f_b\frac{(f_{tb} + \alpha f_m)}{U_u(f_{tb} + \alpha f_b)}, \tag{8}$$

where f_b and f_{tb} are the compressive and the tensile strength of the brick, respectively, f_m is the mortar compressive strength, $\alpha = \frac{h_m}{4.1h_u}$ and U_u is a uniformity coefficient equal to 1.5.

After the peak, the softening behavior under compression is described by a parabolic/exponential softening rule and depends on the fracture energy $G_{f,c}$, considered according to the equation provided by CEB-FIP 1993 (Comite Euro-International du Beton 1993) for concrete:

$$G_{f,c} = 15 + 0.43f_c - 0.0036f_c^2. \tag{9}$$

The dilation effect is also included in the model (van Zijl 2004) by using the parameter:

$$u_p = \frac{\Psi_0}{\delta}\left\langle 1 - \frac{\sigma}{\sigma_u}\right\rangle\left(1 - e^{-\delta\cdot v_p}\right). \tag{10}$$

The initial dilatancy Ψ_0 (without confining stress and shear slip), the confining (compressive) stress σ_u at which the dilatancy becomes zero, and the dilatancy shear slip

degradation coefficient δ are material parameters calibrated trough experimental test data found in literature (Van der Pluijm 1997; Pluijm 1999).

The purpose of this approach is to concentrate all the damage in the relatively weak mortar joints and in the brick interfaces, placed vertically in the middle of each brick. Considering the formulation by Lourenço and Rots for the joint interface behavior (Lourenço and Rots 1997), the following stiffness interface coefficients k_n and k_s are considered:

$$\begin{aligned} k_n &= \frac{E_b E_m}{h_m(E_b - E_m)} \\ k_s &= \frac{G_b G_m}{h_m(G_b - G_m)}, \end{aligned} \tag{11}$$

where E_b and E_m are the elastic moduli of the bricks and of the mortar, respectively, G_b and G_m are the shear moduli of the bricks and of the mortar, respectively, and h_m is the actual thickness of the joint. For the shear moduli of both materials the relationship $G = 0.4 \times E$ was considered.

The adopted mesh includes eight-node quadratic elements for the bricks and six-node quadratic elements for brick–mortar and potential brick crack interfaces. An exponential tension softening model was used for the potential brick-crack elements without a specified shear or compression failure criteria (Fig. 3e). This interface element was modelled with large values of normal and tangential stiffness to ensure brick continuity and to avoid the interpenetration. All the geometrical and mechanical properties of the considered elements are reported in Sects. 4 and 5.

3 FRCM model

Similarly to what stated for masonry, the numerical description of the FRCM system can also be performed by following a micro- or macro-modelling approach; many authors (Basili et al. 2016; Wang et al. 2016, 2017) use a macro-modelling approach based on the smeared crack theory, with the assumption of having layers of mortar homogenized with the distributed composite fabric. Consequently, the reinforcement is modelled as fully embedded in the mortar matrix elements, using grid elements present in different FE program libraries, and therefore their displacements and strains are fully coupled (perfect bond) with the host elements (mortar matrix). Strains of the composites are computed from the displacement field of the mortar matrix elements; this strategy is quite simple and straightforward but some relevant aspects concerning the slippage of the reinforcement fabric inside the mortar matrix could be neglected. Other authors (Garofano et al. 2016; Bertolesi et al. 2016) follow the micro-modelling approach, which consists of modelling each single fiber bundle embedded in the mortar matrix individually; a mortar matrix-fiber bundle interface behavior can be introduced by means of a local bond-slip law, allowing for relative slips between the two components of the strengthening system.

In this paper, the micro-modelling approach is used to describe the FRCM system behavior, allowing for relative slips between the fiber bundles and the mortar matrix. In particular, the formers are introduced as grids of 1D elements, connected to the continuum 2D elements representing the mortar matrix by making use of bond-slip reinforcement interfaces. More in detail, the fiber bundles are modelled as 2-noded linear trusses connected by line-shell interface elements to the mortar matrix in which they are located (Fig. 4). Trusses representing the fibers are considered elastic in tension and not effective in

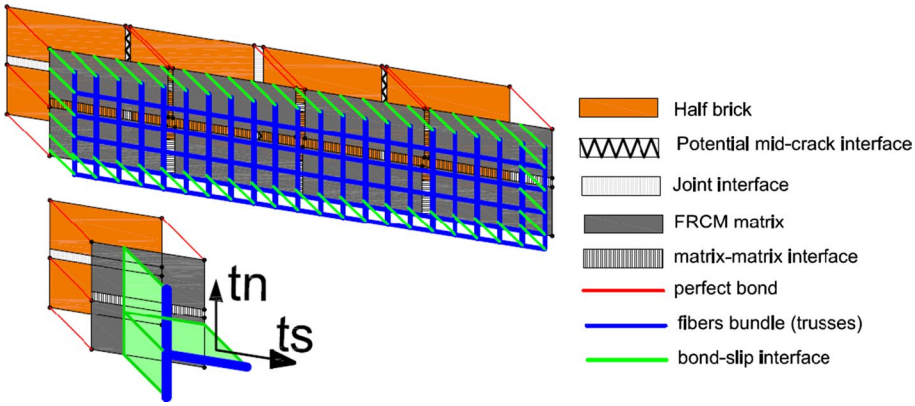

Fig. 4 FRCM strengthened masonry panel: FE model approach and zoom of a cell

compression. The use of a linear elastic behavior for the truss elements is a simplification adopted also for fiber reinforced polymers (FRPs) and verified and supported by experimental evidences (Grande et al. 2008). The bond-slip model adopted, within the software DIANA FEA, sets a non-linear relation between the shear stress and the shear slip, while the relation between normal traction and normal relative displacement is maintained linear, as will be explained in Sect. 3.1. The proposed approach is mainly based on the following outcomes emerged from the experimental tests and from several preliminary numerical calibrations carried out.

The mortar matrix, composed of 2D elements, is introduced in the model as perfectly bonded to the masonry panel, since experimental tests available in literature (Parisi et al. 2013; Corradi et al. 2014) never showed failure modes related to this type of detachment nor suggested the relevance of a possible shear slip between the two systems. In relation to the previous assumption, the mortar matrix substrate is allowed to crack together with the masonry, in correspondence of the same weak locations: mortar bed joints and at mid-brick cross sections. To this purpose, the mortar matrix mesh is made coincident with the masonry mesh, introducing the same potential discontinuities (cracks) trough zero-thickness non-linear interfaces (Fig. 4). These interfaces are modelled using the combined cracking-shearing-crushing material model that has been already thoroughly discussed. Only the definition of normal and tangential interface stiffnesses is modified, considering the presence of only one material (mortar matrix): $k_n = E/t$ and $k_s = G/t$ where E, G are the elastic and shear moduli and t is the thickness of the mortar matrix. Since a 2D mesh is used for the mortar matrix, t is introduced as the overall thickness of the mortar (inner and outer layers included).

3.1 Fiber-mortar matrix interface model

When dealing with FRCM strengthened masonry panels, the interaction between the reinforcement system and the substrate is highly complex and different failure modes are possible, as shown in Fig. 5 (Ascione et al. 2015); among them, the most common are: delamination at the fiber- mortar matrix interface (Fig. 5c), fiber slippage within the mortar matrix with cracking of the outer layer of the mortar (Fig. 5e) and tensile rupture of the fibers (out of the bonded area—Fig. 5f). For reasons of simplicity, all the delamination and slippage

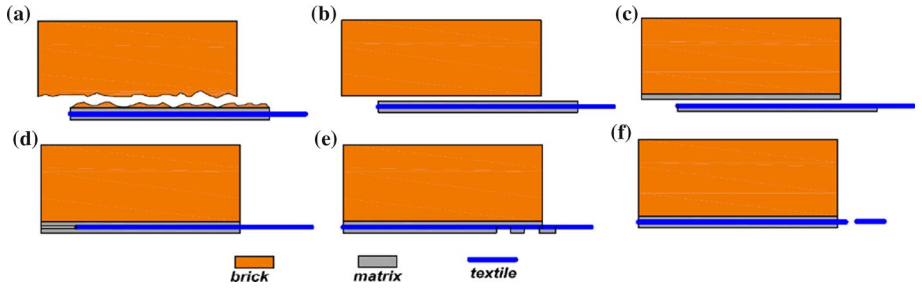

Fig. 5 Possible failure modes for externally bonded FRCM systems applied on a brick masonry substrate: **a** debonding with cohesive failure in the substrate, **b** delamination at the FRCM-to-substrate interface, **c** delamination at the fiber-to-mortar matrix interface, **d** fiber slippage within the mortar matrix, **e** fiber slippage within the mortar matrix with cracking of the outer layer of mortar, **f** tensile rupture of the fibers

phenomena are concentrated at the fiber bundle-mortar matrix interface. The latter being by far the most frequent mechanism leading to failure, after the rupture of the fibers, which is not considered here since it can be explicitly taken into account by the fiber model.

The potential slippage of the fiber bundles with respect to the mortar matrix is described by zero-thickness interface elements with six-nodes, a quadratic displacement field and a plane stress assumption. Since they connect 1D elements (fiber bundles) to 2D shell elements (mortar matrix layer), two separate interface laws are assigned along the longitudinal direction and along the direction orthogonal to the fiber bundle alignment. The adopted constitutive laws are based on a total deformation theory, which expresses the stresses as a function of the total relative displacements.

The relation between the normal traction and the normal relative displacement is assumed to be linear elastic and characterized by the k_n stiffness. The large deformability of fibers along the direction orthogonal to their alignment and the possibility of relative slippage between orthogonal bundles, suggest that a negligible value of the k_n stiffness should be considered. Therefore, a very weak stiffness (Fig. 6a) is given to the bond-slip interface elements along the direction orthogonal to the fiber bundles, to neglect their contribution along that direction. This is particularly important for the fibers placed along the wefts, i.e. in the direction orthogonal to the application of the force (Fig. 6c). A parametric analysis is carried out to verify the role of the k_n stiffness, obtaining that with non-negligible values of k_n (i.e. values larger than unity) the force-slip relationship is enormously overestimated.

A bilinear shear stress-slip numerical curve is considered along the longitudinal direction; this is a simple but common choice for FRCM systems (Bertolesi et al. 2016). More sophisticated models could have been used but given the purpose to perform structural analysis with a large number of interface elements and the growing difficulty of calibrating increasingly complex laws, the choice seems appropriate. Shear laws for positive and negative values of slips are equal.

In order to calibrate the considered interface laws and to verify the simplified assumptions introduced, some finite elements numerical simulations of available experimental bond tests between FRCM and bricks are carried out. In more details, experimental bond tests performed on Carbon-FRCM systems (Carozzi et al. 2017) applied on single bricks are numerically modelled considering three different mechanical properties of the constituent materials and geometries of the fibers. The different FRCM systems investigated are here denoted as: Carbon 1, Carbon 2 and Carbon 3. They are all made of balanced

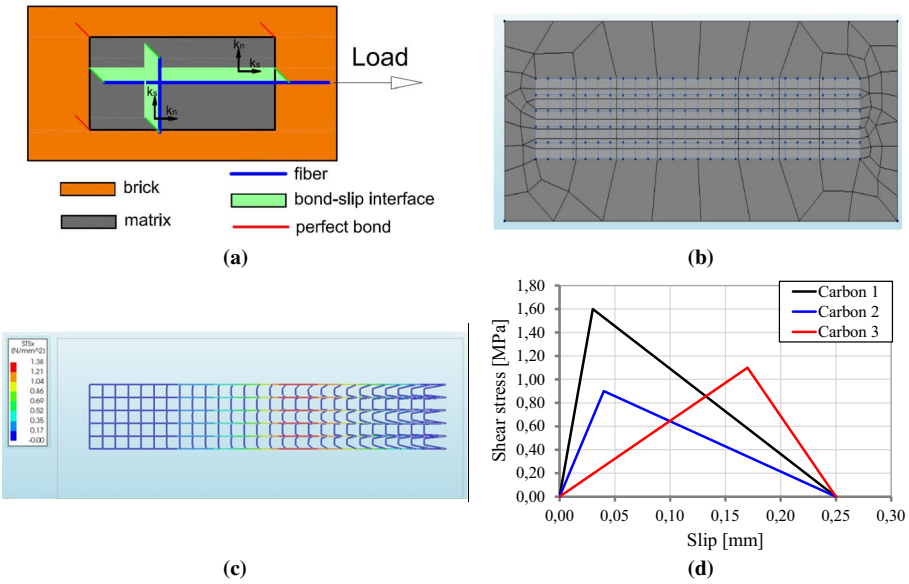

Fig. 6 Numerical simulations of bond tests: **a** numerical modeling, **b** numerical mesh, **c** contour plot of the shear stresses along the fibers at peak, **d** bond-slip constitutive laws

bidirectional carbon fiber grids embedded in a lime-based mortar matrix (Carbon 1) or a cementitious mortar matrix (Carbon 2 and 3), having the mechanical properties reported in Table 1. In general, it can be stated that the bond behavior of FRCM systems can be strongly dependent on the type of fibers, on the mortar matrix properties and on the interaction between the constituents, both from the mechanical and the chemical point of view. In the numerical analyses of bond tests, to improve the validity of the chosen numerical approach, a variety of carbon FRCM systems is considered. The geometrical properties of

Table 1 Numerical simulations of bond tests: mechanical and geometrical properties of the specimens

Property	Units	Carbon 1	Carbon 2	Carbon 3
Brick dimensions	mm	125×120×315	125×120×315	250×120×315
Bond length	mm	260	260	260
Bond width	mm	54	50	100
Number of yarns (warp)	–	6	5	10
Number of yarns (weft)	–	29	25	26
Mortar matrix thickness	mm	12	10	9
Yarn section	mm^2	0.47	0.47	0.47
Yarn perimeter	mm	4	8	8
Grid spacing	mm	10	10	10
E_{fiber}	GPa	240	197	203
E_{matrix}	GPa	8	7	7
Matrix compressive strength	MPa	9.8	20	20
Matrix flexural strength	MPa	3.8	6.7	6.7

the brick substrate and of the FRCM systems are reported in Table 1: the bond length is the same while a different configuration of bond width and number of yarns is considered. In the cited experimental program (Carozzi et al. 2017), the prevalent failure modes registered are delamination at the fiber-mortar matrix interface (Fig. 5c) and slippage of the fibers within the mortar matrix (Fig. 5d, e).

For the calibration of the bond-slip laws, non-linear analyses are performed with the finite element software DIANA FEA 10.1. In the numerical simulations, the brick is considered as a linear elastic material and the FRCM system is modelled as previously exposed (Fig. 6a, b). To simulate the bond tests, the free edges of the fiber bundles (truss elements) were pulled horizontally by imposing a common displacement, while restraining the brick substrate. The typical trend of the interface shear stresses in a bond test, obtained at peak from the numerical simulation referred to the Carbon 1 strengthening system, is presented in Fig. 6c. The numerical results of the bond tests in terms of axial stress *vs* slip curves are shown in Fig. 7, in which the axial stress is evaluated as the applied force divided by the cross section of the dry fibers. Trying to capture the maximum displacement capacity for the Carbon 2 strengthening system, the results of the numerical analysis are shown also for the post-peak phase, even if, due to convergence issues, they can be characterized by a limited reliability in the last branch of the curve. The calibration of the bilinear bond-slip laws is performed by direct comparison and fitting of the experimental results described in (Carozzi et al. 2017), where only the failure mode associated with slippage of the fibers within the mortar matrix is included according to the results of experimental tests and literature evidences (Nerilli and Ferracuti 2018; Grande and Milani 2018).

Figure 7 shows a good matching between numerical axial stress versus slip curves and experimental envelopes, for all the FRCM systems. In particular, initial branches of

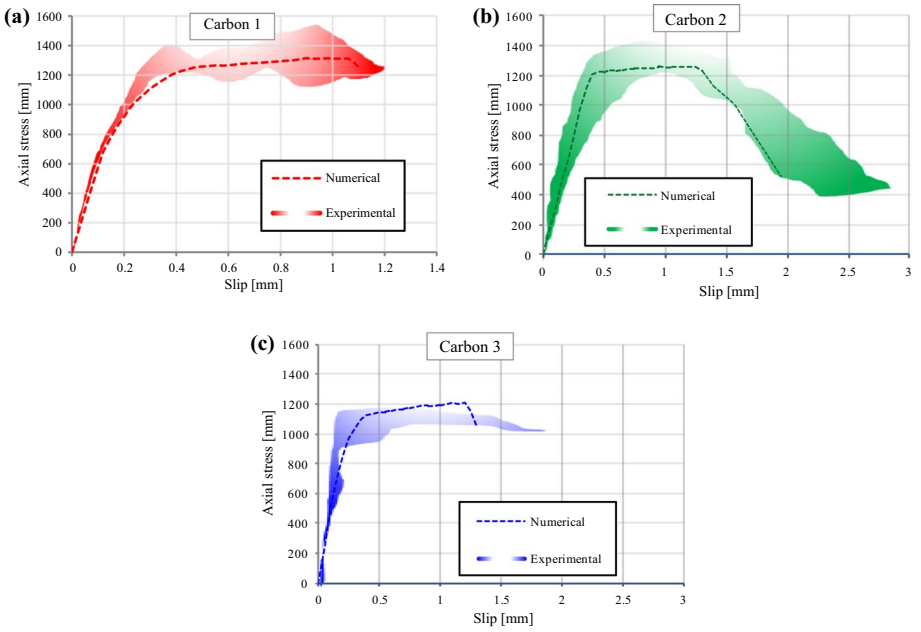

Fig. 7 Comparison between experimental results and numerical simulations of bond tests on Carbon FRCM systems: **a** Carbon 1, **b** Carbon 2 and **c** Carbon 3

numerical curves are very similar to the experimental ones and a satisfactory matching in terms of peak force was obtained; in fact, all numerical predictions fall in the middle of the experimental range of values. This confirms the suitability of the adopted modelling choices. Parameters describing the bilinear bond-slip laws, in terms of maximum shear stress τ_{max}, shear slip at peak s_{peak} and ultimate shear slip s_u, are reported in Table 2 while their graphical representation is reported in Fig. 6d.

Parametric analyses are performed for the bond tests with the Carbon 1 strengthening system, by varying the main parameters governing the bilinear bond-slip laws as reported in Table 3. In more detail, variations in terms of peak shear stress and initial stiffness were considered. The results of the parametric analyses are reported in Fig. 8 in terms of axial stress *vs* slip: it can be noticed that the variations of peak shear stress are correlated to variations in terms of initial stiffness and higher capacities, in terms of strength and displacements, are associated to higher peak shear stress.

Table 2 Calibrated bond-slip laws

Property	Units	Carbon 1	Carbon 2	Carbon 3
τ_{max}	MPa	1.6	1.1	0.9
s_{peak}	mm	0.03	0.17	0.04
s_u	mm	0.25	0.25	0.25

Table 3 Bond-slip laws: parametric analyses

Property	Units	Carbon 1 (best bond)	Carbon 1 (medium bond)	Carbon 1 (weak bond)
τ_{max}	MPa	4.8	2.4	0.55
s_{peak}	mm	0.03	0.03	0.03
s_u	mm	0.25	0.25	0.25

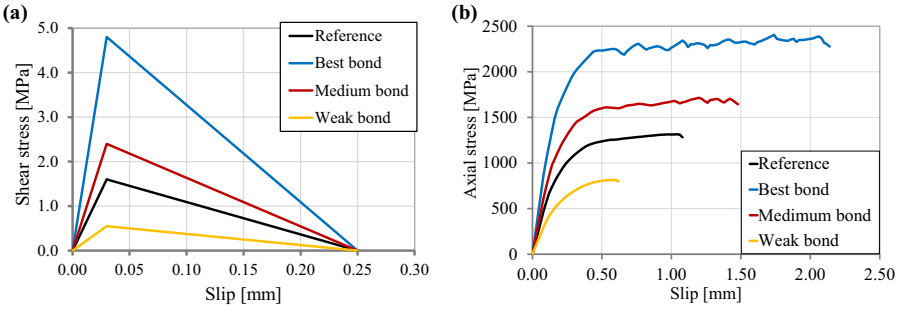

Fig. 8 Parametric analyses of bond tests on the Carbon1 strengthening system: **a** adopted bond-slip constitutive laws, **b** axial stress versus slip curves

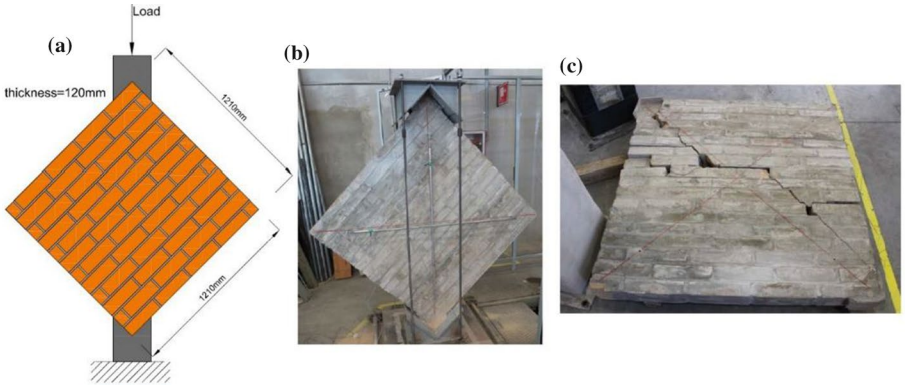

Fig. 9 Diagonal compression test: **a** geometrical properties of the panel, **b** experimental unreinforced panel and set-up, **c** unreinforced panel failure mode

Table 4 Mechanical properties of considered materials from tests

Property	Units	Brick	Mortar (joint)	FRCM matrix	Fiber
E	GPa	14	7	17	240
f_c	MPa	44	8	5	–
f_t	MPa	5	3	3	2400

4 Reference experimental tests

To evaluate the effectiveness of the proposed numerical approach at a structural level, some diagonal compression tests on unreinforced and reinforced masonry walls are considered (Ferretti et al. 2016, 2017) and simulated. In the cited experimental programs, the masonry panels were laid in a single-leaf running bond pattern, with a final dimension of $1210 \times 1210 \times 120$ mm^3 (Fig. 9a). They were built with fired clay bricks and cementitious mortar, with 10-mm thick mortar joints. The panels were also strengthened with different FRCM systems: the case of bidirectional carbon grid embedded into a lime-based mortar matrix is analyzed in the present paper. The type of reinforcement coincides with one of the systems previously considered for the calibration of the bond-slip laws and, in particular, with the Carbon 1 strengthening system, whose properties are reported in Table 1.

The procedure for the strengthening of the panels by means of the FRCM system was typical. It consisted in: applying a first layer of mortar matrix to both surfaces of the panel, placing the bidirectional carbon grid over the mortar matrix and partially embedding the grids inside it; finally, a second thin mortar layer was cast on both sides of the panel. The final thickness of the strengthening system (on each side of the panel) was equal to 6 mm. The mechanical properties of the constituent materials, derived from the results of the cited experimental campaigns, are summarized in Table 4 in terms of elastic modulus E, compressive strength f_c and tensile strength f_t.

The diagonal compression test consisted in applying a compressive vertical load along one diagonal of the square panels. During the tests, the vertical and horizontal deformations were measured by means of 2 vertical and 2 horizontal displacement

transducers, which measured the shortening of the compressed diagonal of the panel and the elongation of the diagonal under traction, respectively (Fig. 9b). Tests were conducted under force control until the peak and then under displacement control.

Figure 9c shows the failure mechanism of one unreinforced masonry panel, which was characterized by one main tensile crack along the compressed diagonal; it developed from the center of the wall and it propagated towards the corners crossing both the bricks and the bed and head mortar joints. After the peak load was reached and the diagonal crack completely formed, the load capacity dropped suddenly to zero with a very brittle failure (Fig. 10).

The application of the FRCM strengthening system increased the capacity (+30%) and improved the post-peak behavior (Fig. 10), leading to a more ductile failure mode with respect to the one of the unreinforced panels. Moreover, the presence of the FRCM system inhibited the formation of one single predominant crack, better distributing the damage and the cracks over a wider portion of the panels. At the end of the tests, indeed, multiple cracks were visible both on the external surface of the FRCM strengthening systems and in the masonry substrates (Fig. 11). The FRCM system failed mainly due to delamination at the fiber-mortar matrix interface, similarly to what observed in the bond tests.

5 Model material properties and boundary conditions

The main mechanical properties of the materials used in the numerical analyses are obtained from the experimental tests (Ferretti et al. 2016, 2017) and are reported in Table 4. The adjusted dimensions of the single brick are $120 \times 250 \times 55$ mm^3 ($L \times B \times H$). All the other parameters defining the behavior of the brick–mortar interface and of the interfaces within the mortar matrix are evaluated according to the general values found in literature (Lourenço 1996; Rots 1997; Lourenço and Rots 1997) and on the basis of the experimental tests presented in previous researches (Masia et al. 2006; Petersen 2009). They are reported in Table 5. According to an experimental

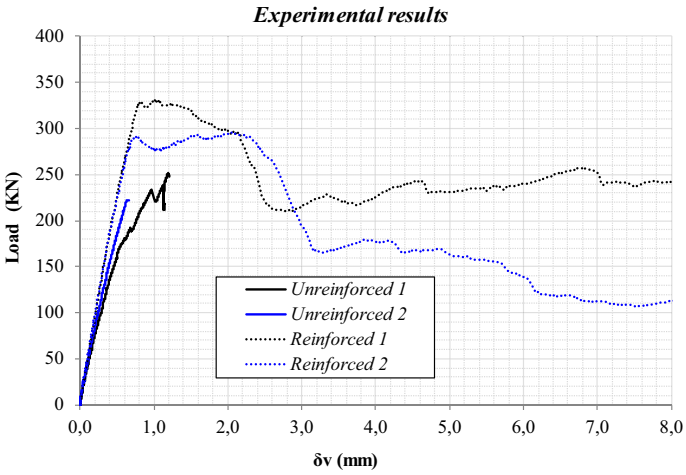

Fig. 10 Experimental tests: comparison of unreinforced and reinforced panel results in terms of force–displacement curves

Fig. 11 Diagonal compression test: failure mode of the FRCM strengthened samples

campaign conducted on masonry columns made by the same materials (Incerti et al. 2015), the longitudinal deformation at peak under compression is considered equal to 0.44%. The interface element describing the potential crack inside the bricks is governed by a non-linear curve made of an initial linear elastic branch followed by an exponential softening behavior with a tensile strength of 3 MPa and a fracture energy of $G_f^{\mathrm{I}} = 0.025$ N/mm, based on the recommendations from Lourenço (Lourenço 1996). The optimal values of the parameters governing the non-linear fiber-mortar matrix interfaces are obtained in the previous phase (Sect. 3.1) from the numerical simulations of bond tests on the FRCM system denoted as Carbon 1, since the materials were exactly the same.

In accordance with experimental tests, in the numerical models, the FRCM composite is applied to the masonry surfaces adopting an offset of about 20 mm from the lateral edges, to prevent the direct application of the force to the reinforcement layer, which could trigger early delamination phenomena. The boundary conditions and loading scheme are set according to the real test conditions (Fig. 12). Numerical analyses are carried out under displacement control. The vertical displacement along the compressed diagonal is assigned through two steel cradles (properly meshed) placed at two opposite corners of the panels. The contact surfaces between the panel and the cradles are also modelled trough interface elements since this aspect proved to be significant for the capacity of the panel (confining effect of the corners) and the cracks distribution and initiation. The normal stiffness of the interface was high (10^8 N/mm^3) in order to avoid interpenetration while a small tangential stiffness value (450 N/mm^3) was calibrated to allow relative displacements and to properly simulate the friction between the steel shoes and the masonry panel and, consequently, the confinement at the corners. With the chosen values, the ratio between the maximum shear and normal stresses along the interface is almost constant during the analyses and equal to 0.3.

Table 5 Mechanical parameters of the interface elements

Interface	$k_n\left(\frac{N}{mm^3}\right)$	$k_t\left(\frac{N}{mm^3}\right)$	f_t (MPa)	$G_f^I\left(\frac{N}{mm}\right)$	$c\left(\frac{N}{mm}\right)$	ϕ_0 (rad)	ϕ_r (rad)	$G_f^{II}\left(\frac{N}{mm}\right)$	Ψ_0 (rad)	σ_u (MPa)	δ (–)	f_c (MPa)	C_s (–)	$G_{f,c}\left(\frac{N}{mm}\right)$	κ_p (–)
Brick–mortar	1350	550	0.25	0.001	0.40	0.85	0.85	0.05	0.75	−2	5	17	9	21	0.0044
FRCM matrix–matrix	2000	800	3.00	0.025	0.55	0.85	0.85	0.10	0.75	−2	9	5	9	17	0.0013

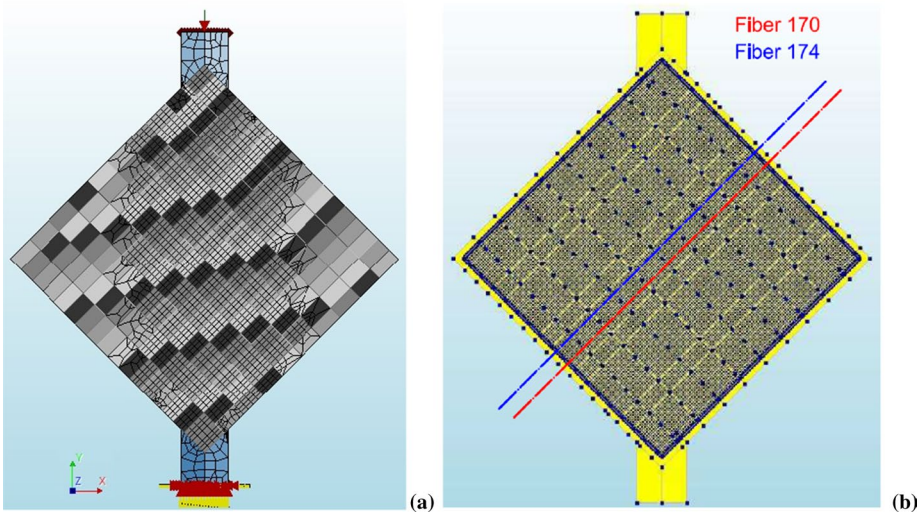

Fig. 12 In-plane FE masonry model: **a** unreinforced panel, **b** FRCM strengthened panel

6 Numerical results and discussion

In this section, numerical outcomes coming from the analyses of both unreinforced and FRCM strengthened masonry panels are presented, discussed and compared with the corresponding experimental results. In particular, after the calibration of the key parameters by using suggested literature procedures and results from simulation of bond tests (as discussed before), the modelling strategy was validated by comparing numerical and experimental results, not only in terms of mechanical curve but also of cracking pattern and failure mode.

6.1 Unreinforced masonry panel

The numerical load-vertical shortening (δ_v) curve of the unreinforced masonry panel is shown in Fig. 13a, together with the experimental counterparts (two identical tests). The numerical curve fits quite well the experimental outcomes, closely matching the mean strength value and the corresponding shortening obtained from the two experimental tests. The initial stiffness of the system is properly captured as well as the beginning of the non-linear branch (around 85% of the peak load). The experimental post-peak behavior was not properly registered due to the fragility of the experimental failure.

The numerical failure is governed by the formation and development of one main crack along the compressed diagonal (Fig. 14), in good accordance with the experimental evidences (Fig. 9c). Taking into account the unavoidable scattering of experimental results, the prediction capability of the numerical model can be considered as quite satisfactory.

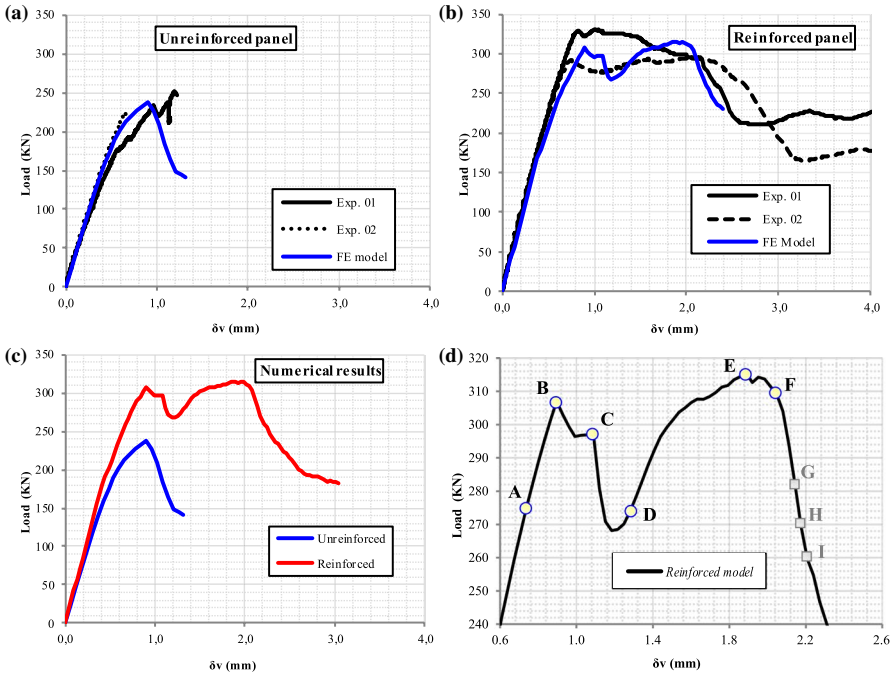

Fig. 13 Comparison of experimental and numerical results: **a** unreinforced panel, **b** FRCM strengthened panel, **c** numerical unreinforced versus reinforced panel behavior, **d** zoom of the reinforced model

6.2 FRCM strengthened masonry panel

Figure 13b shows the comparison between the numerical and experimental load-vertical shortening curves related to the FRCM strengthened masonry panels. As before, the initial stiffness is properly captured but the experimental curves show slightly less non-linearity before reaching the first peak. The numerical model is then capable of describing the second peak with a good matching of both values of maximum loads, which were similar for both tests. Also in terms of vertical shortening (δ_v), the prediction is realistic and inside the experimental range.

As clearly shown in Fig. 13c, the FRCM strengthened masonry panel experiences a significant increase (+30%) in the load bearing capacity with respect to the unreinforced one, confirming the experimental outcomes (Fig. 10). At the same time, the presence of the FRCM reinforcement improves the failure mechanism, bridging the main crack and allowing for an effective stress redistribution, which leads to the formation of multiple cracks before failure (Fig. 15). Correspondingly, the post-peak behavior is less brittle (Fig. 13c) and the sample is allowed to reach much greater deformations before failure.

In terms of initial stiffness, the FRCM strengthened masonry panel does not provide for a strong increase with respect to the unreinforced one, since the thickness of the mortar matrix layers is small (6 mm only). Nevertheless, the positive effect of the application of the strengthening layers on the masonry becomes particularly evident for high load level, when the smaller cracks opening into the masonry allows for a reduced non-linearity and a greater load capacity.

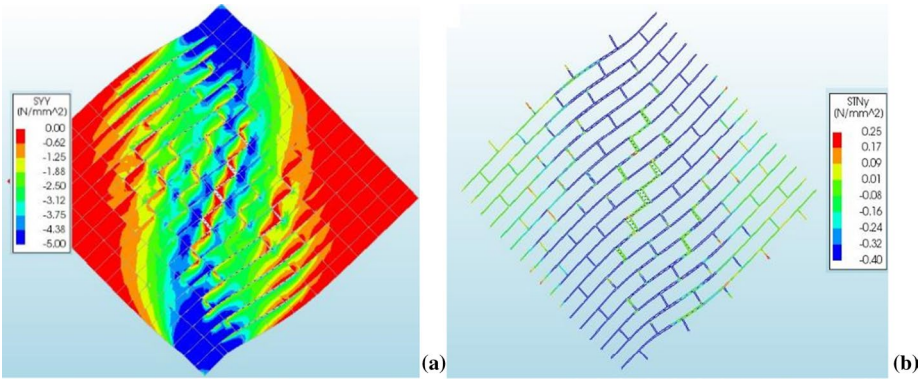

Fig. 14 Numerical results for the unreinforced panel at peak: **a** vertical stresses on the brick elements, **b** joint interface normal stresses

From the numerical results, the mechanical behavior of each single component of the FRCM strengthened panel can be observed and described. In particular, considering the reference points highlighted in Fig. 13d (A to I), describing the typical load-vertical shortening curve of the FRCM strengthened panel, the event leading to the reaching of each point and the corresponding responsible FRCM component can be identified as follows:

A. The masonry panel is at the end of its elastic phase since the first crack begins to appear locally inside it while the external mortar matrix layer is usually still uncracked. However, cracks do not compromise the stability of the panel, which continues to bear load increments.
B. Diffused masonry cracking happens, although there were FRCM layers still uncracked that covers it.
C. Some macro-cracks start appearing into the mortar matrix and, correspondingly, fibers bridging them reaches the peak shear stress (1.6 MPa in the present case) and the onset

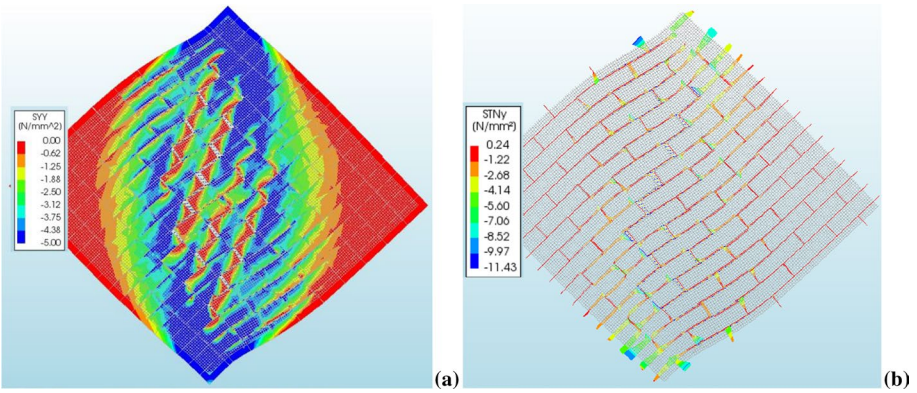

Fig. 15 Numerical results for the FRCM strengthened panel (load step corresponding to point C of Fig. 13d): **a** masonry failure pattern and stresses on the bricks, **b** joint interface normal stresses

of local delamination. At this step, the amount and type of mortar matrix and fibers can be important for the definition of the load reduction from B to C.

D. Crack opening and fiber slippage determine the evident force drop, until stress redistribution allows for a proper bonding of fibers, which are actually working alone through the cracks. Until this condition is stable, the system can recover the load.
E. The peak shear stress is reached in correspondence of few further fiber alignments.
F. Bond failure of a significant number of fibers: the extent of stress redistribution is so diffused that fibers do not have the minimum bond length requested and the final failure of the FRCM system (due to delamination) is reached.

The points G, H and I, visible in the graph of Fig. 13d, refer to the very last part of the analyses and will be introduced in Sect. 7.4, which deals with the discussion about the parametric analyses on the amount of fibers.

These findings confirm that the crack pattern and failure mechanism of the FRCM strengthened panels are directly affected by both the fibers and the mortar matrix characteristics. The mortar matrix gives stiffness and peak stress contributions, while the fibers allow to reseal the crack of the masonry panel and then provide for a more ductile post-peak behavior and eventual force recovery (if the bond is effective).

This description of the different phases of the diagonal compression test finds confirmation also in the experimental findings, which showed similar types of peaks, cracking evolution, force recovery and failure mechanisms. In particular, similar crack patterns, involving bricks and mortar joints and characterized by similar orientation, can be noticed by comparing numerical (Fig. 15) and experimental results (Fig. 11). A proper matching was only possible since the bond-slip relationship between fibers and mortar matrix has been introduced inside the numerical model together with the possibility for the mortar matrix to crack.

6.3 Shear stress redistribution along the fibers

In order to investigate the delamination process of the composite fibers within the mortar matrix during the test, two representative fiber bundles are considered, positioned in the middle of the FRCM strengthened masonry panel (red and blue dash-dot lines in Fig. 12b). For each one of them, the shear stress distribution along the fiber at different imposed vertical shortening, corresponding to the B-F points in Fig. 13d, is shown in Fig. 16a, b for

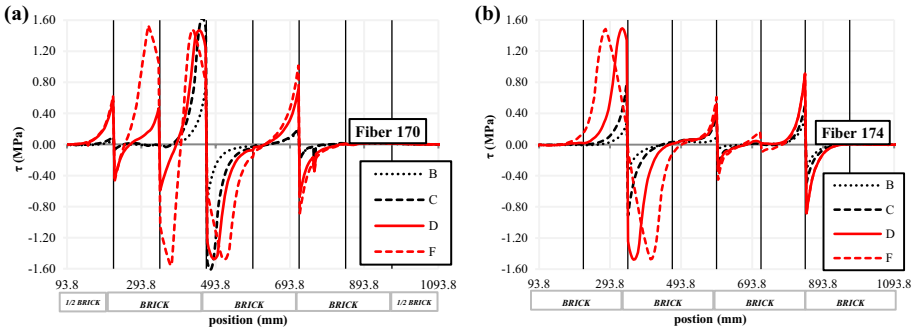

Fig. 16 Shear stress distributions along **a** fiber 170 and **b** fiber 174

fiber 170 and 174, respectively. The vertical black lines in the graphs represent the potential discontinuity inside the masonry due to the presence of the head joints or the crack surfaces modelled inside the bricks. In order to recognize the specific role of each vertical line, a sketch of the bricks along the fiber bundles is reported at the bottom of the graphs.

Considering the behavior of the fiber bundle 170 (Fig. 16a), when the mortar matrix starts cracking (point B in Fig. 13d), in some cross-sections (head joints) a remarkable increase of shear stress can be found, which reaches the shear strength at the formations of macro-cracks (point C of Fig. 13d). In the following steps, the shear stress peak shifts away from the head joints (e.g. position 493.8 mm) due to the development of the delamination process. When a new crack inside the brick develops (line D at position 293.8 mm), a sudden delamination is observed with a subsequent shear stress redistribution (line F) towards portions of the bundle less stressed.

A similar behavior can be observed for the fiber bundle 174 (Fig. 16b), where the onset of delamination (position 293.8 mm) is reached at a later stage (point D of Fig. 13d) due to the different position of the bundle inside the masonry panel; moreover, the shift of the shear stress diagram is much larger than in the previous case and crosses the half-brick interface without any discontinuity, since there is no crack there. In the following steps of the analysis (not reported for brevity), that diagram keeps moving towards the edge of the bundle and once it reaches the minimum bond length, the bundle fully delaminates. Since this condition is reached at different time instants for each bundle or it is never reached if the bond failure happens before (fiber bundle 170), a certain force redistribution is possible among the bundles; at a macroscopic level, this can be associated with the descending branch of the curve, after point F (Fig. 13d). A FRCM strengthened masonry panel can exploit this important resource during its non-linear post-peak behavior, depending on the quality of the fiber-mortar matrix bond.

7 Parametric analyses

After validating the proposed numerical model for the description of masonry panels strengthened by FRCM systems, the model is used to investigate the relevance and the importance of the main parameters and their influence on the overall structural response. In particular, the proposed 2D FE model of the FRCM strengthened masonry panel is used to develop parametric analyses for investigating the effect of the main geometrical and mechanical parameters of the strengthening system, with particular attention to the effects on the non-linear behavior and the failure mode.

The analyses involve two different groups of parameters, the first being related to the following mechanical properties: elastic modulus and tensile strength of the mortar matrix, shear strength τ_{max} (with a constant slip at peak $s_{peak} = 0.03$ mm) and shear slip at peak s_{peak} of the bond-slip relationship at the fiber-mortar matrix interfaces. The second parameter's group concerns the amount of fibers embedded inside the mortar matrix; the case of mortar matrix without fibers is also considered.

Table 6 shows the values considered for the mechanical parameters; the adopted approach is to change one parameter at a time, at least for the parameters explicitly considered. The combination of the parameters used to match the experimental tests described in Sect. 5 is referred to as *Ref*. The considered range of variability of the elastic modulus of the mortar matrix covers adoption of soft mortars and of thick mortar layers: the cross section of the mortar matrix is indeed kept constant in the model and the membrane stiffness

Table 6 Parametric analyses: combinations of mechanical parameters for the FRCM strengthened masonry panel

Property	Units	Ref	Soft	Stiff	Weak	Strong	Best bond	Medium bond	Weak bond	s_{peak}
$E_{FRCM,matrix}$	GPa	17	5.5	51	17	17	17	17	17	17
$f_{t,FRCM,matrix}$	MPa	3	3	3	1	6	3	3	3	3
τ_{max}	MPa	1.6	1.6	1.6	1.6	1.6	4.8	2.4	0.55	1.6
s_{peak}	mm	0.03	0.03	0.03	0.03	0.03	0.03	0.03	0.03	0.15

is properly modified trough the variation of the elastic modulus only. The mortar matrix tensile strength is varied within a realistic range which can be easily found in literature (Leone et al. 2017; Carozzi et al. 2017) and considers also a possible degradation of the mortar itself. Finally, the shear strength of the interface law ranges from low values, found when dry fibers and non-compatible mortar matrix are used, to high values, which can be found when adhesion promoters or epoxy addition are adopted within the mortar matrix. In particular, the values of the shear strength in the parametric analyses are taken coherently with the values presented in Sect. 3.1 for the bond tests by considering multiples of the reference value of τ_{max}. In this perspective, the combinations included in Table 6 can be considered realistic (Leone et al. 2017; Carozzi et al. 2017).

Table 7 shows all the considered amounts of strengthening fibers, described in terms of cross section and wet perimeter. Fiber densities ranging approximately from 80 g/m^2 to 500 g/m^2 are considered, as can be found in the market. In the last row of Table 7 (double layer), the cross section is increased but the bond capacity (wet perimeter) of the system remains the same.

7.1 Effect of mortar matrix properties

Figure 17a shows the load-vertical shortening curves of FRCM strengthened masonry panels with different elastic modulus of the mortar matrix ($E_{FRCM,matrix}$). As expected, the larger the value, the larger the stiffness of the initial uncracked branch. A large deformability of the mortar matrix (*soft curve*) leaves the masonry alone in the definition of the first peak, which is then remarkably reduced with respect to other cases (*ref.*, and *stiff*); on the contrary, a too stiff mortar matrix (*stiff*) cracks before the masonry, leaving almost unaffected the stress at first peak. Intermediate cases have the same first peak and type of

Table 7 Parametric analyses on the amount of strengthening fibers

Model number	Name	Area (mm^2)	Perimeter (mm)
1	Unreinforced	–	–
2	Only mortar	–	–
3	Ref. model	0.46	4
4	Double density	0.92	5.64
5	High density	1.38	6.92
6	Light density	0.23	2.83
7	Non-struct. fiber	0.115	2
8	Double layer	0.92	4

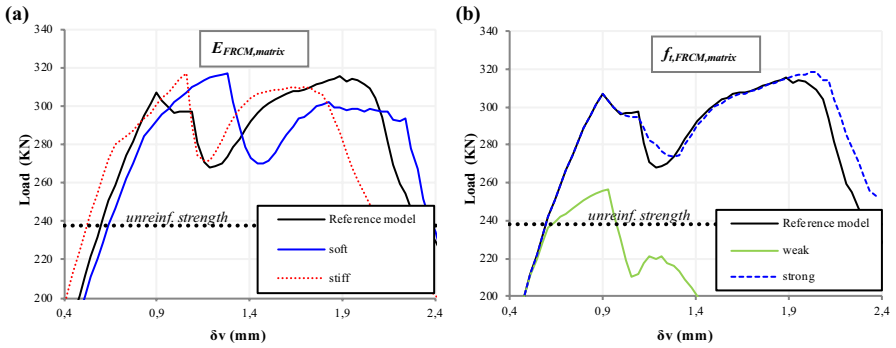

Fig. 17 Parametric analyses: effects of variation of **a** elastic modulus of the mortar matrix and **b** tensile strength of the matrix

behavior, since the sequence of cracking (masonry and then matrix) and the mortar matrix tensile strength are the same, leading to the formation of several cracks. After the first peak, the mortar matrix stiffness also affects the possibility of having a force recovery, due to some "tension stiffening" mechanism allowing for an effective distribution of cracks around the central portion of the panel.

Figure 17b shows the effect on the shear behavior of the mortar matrix tensile strength; in particular, when using a weak mortar matrix, it cracks before the masonry and produces a sudden knee in the curve, like for curve *stiff* of Fig. 17a, but in correspondence with a much lower force value. Correspondingly, the first peak is of limited intensity and mainly due to masonry capacity (256 kN versus 238 kN of the plain masonry). On the other side, a large increase of tensile strength seems partially un-effective without a comparable increase of elastic modulus, since the first peak is shifted towards larger deformations and crack openings, where the larger mortar matrix force contribution is balanced by the smaller masonry counterpart, clearly inside its softening behavior. Moreover, once the tensile strength is locally reached, the post-peak stress behavior is more brittle and, correspondingly, the global force redistribution capability is reduced. Once the mortar matrix is cracked, the second peak is mainly governed by the amount of fibers and their strength; in fact, *Ref.* and *strong* provided for the same maximum capacity.

7.2 Effect of fiber-mortar matrix bond properties

The influence of the fiber-mortar matrix bond-slip relationship is investigated, by introducing different values of maximum shear stress and slip at peak. While variations related to the slip were not highly relevant, important remarks can be done concerning τ_{max} variation.

Figure 18a shows curves obtained with different values of τ_{max} (Table 6), associated to a corresponding difference in the initial stiffness of the bond-slip relationship; this combined effect leads to a stiffness increase of the final part of the curve leading to the first peak, when increasing their values; nevertheless, the force level localizing this peak or discontinuity did not vary so much (from 305 to 310 kN) since it was mostly related to the mortar matrix properties. A stronger bond delays the mortar matrix cracking, providing for a better compatibility between mortar matrix and fibers. For the same reason, larger τ_{max} (and initial stiffness) values reduced the post-peak

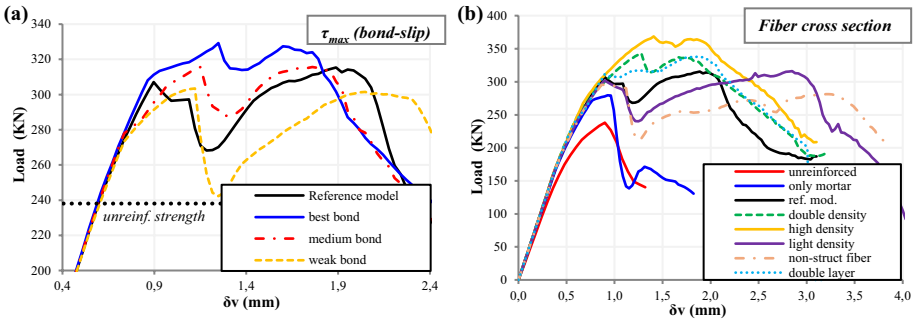

Fig. 18 Parametric analyses: effect of variation of **a** peak shear stress and **b** fiber amount

load drop (see curves *best, medium* and *weak bond*), while the second peak force value (approximately 320 kN) does not change significantly, since it is mainly related to the fibers capacity. In fact, even a poor bond allows for reaching the same final capacity, since fiber bundles are able to find portions of the masonry panel around the main cracks where to properly transmit the bond stresses. This is something that cannot be observed through a simple bond test but specimens with variable stress levels are required. Finally, a growing bond capacity (and initial bond stiffness also) leads to a force recovery branch (at the beginning of second peak) of increasing slope, to a smaller deformation at second peak (from 2.1 to 1.6 mm) and to an increase of brittleness at failure.

7.3 Variation of amount of fibers

Figure 18b shows the shear behavior of FRCM strengthened masonry panels with different amount of strengthening fibers (see Table 7). As expected, the application of mortar matrix only produces an increase of stiffness and shear strength (with respect to the unreinforced case) but a very brittle failure occurs. The introduction of a growing amount of fibers inside the mortar matrix does not improve the first peak so much, since before cracking mortar matrix is more effective than fibers. Only when the amount of fibers is relevant (double density and high density) and properly bonded, the initial capacity is remarkably enhanced, even because the mortar matrix is thin. In fact, when two layers of strengthening grids are considered (double layer), first peak is not so affected and the effect of fibers can be observed only later, because of the limited bond between mortar matrix and fibers.

The force drop after the first peak and the slope of the following force recovery branch (*tension stiffening effect*) are strongly related to the amount of fibers: the former being inversely dependent and the latter being proportional to it. This can be explained by considering the better stress redistribution which takes place around the main cracks with growing amount of fibers. As a consequence, a stronger reinforcement tends to merge the two peaks into one (from non-structural to high density). Table 8 summarize the force and vertical shortening peak values for the considered configurations, with the corresponding relative increments. The second peak is only provided for strengthened masonry panels.

Table 8 Results of the parametric analyses

Name	P_1 (kN)	ΔP_1 (%)	d_1 (mm)	Δd_1 (%)	P_2 (kN)	ΔP_2 (%)	d_2 (mm)	Δd_2 (%)
Unreinforced	238	–	0.90	–	–	–	–	–
Only mortar	270	13	0.96	6	–	–	–	–
Ref. model	307	29	0.90	0	313	–	1.98	–
Double density	343	44	1.28	42	335	7	1.79	− 10
Hingh density	368	55	1.41	56	364	16	1.86	− 7
Light density	301	26	0.90	0	313	0	2.88	45
Non-struct. fiber	299	25	0.90	0	280	− 11	3.17	60
Double layer	312	31	0.90	0	337	7	1.86	− 7

7.4 Discussion about parametric analyses

Some of the previous findings are confirmed by the shear stress distributions along the fiber 170 reported in Fig. 19, where each curve represents a different imposed vertical shortening, corresponding to the δ_v value of B–F points in Fig. 13d. Shear stress distribution curves associated with a τ_{max} variation are consistent with the previous remarks: high value of τ_{max} and consequently also of the stiffness (Fig. 19b) produces a more

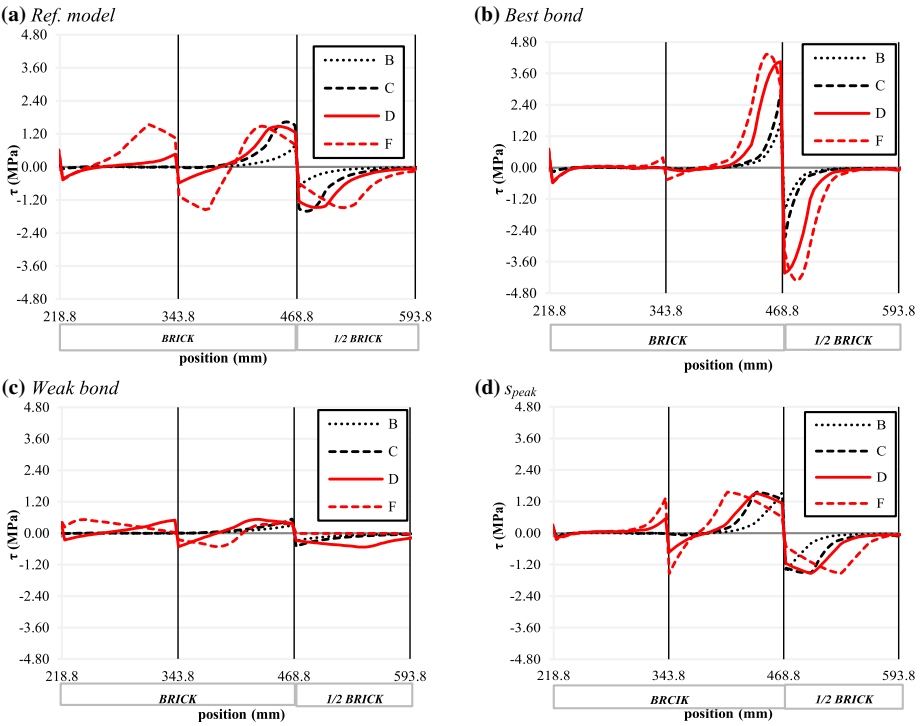

Fig. 19 Shear stress distributions along the fiber 170 for the numerical models reported in Table 6

rigid behavior; on the contrary adopting a softer bond-slip law (Fig. 19c), shear stress peak shifts away quickly and over a long distance.

Figure 19d shows the shear stress distribution for the model in which the s_{peak} was half the value considered in the *Ref.* case; as expected, the onset of delamination was reached before the *Ref.*, at δ_v value corresponding to point B, and during delamination a shear stress diagram with larger slopes can be found.

In Fig. 20, axial and shear stress distributions along the fiber 170 are reported for masonry panels strengthened with half or three times the amount of fibers. In these graphs, further δ_v steps have been added (G to I points in Fig. 13d) to better investigate the stress redistribution at large displacements, corresponding to the ultimate points of the analyses. With reference to the shear stress distributions (Fig. 20b, d), it can be noticed that when the amount of fibers is reduced (light density), delamination starts sooner and it leads more rapidly to the final failure: by imposing the same vertical shortening to the masonry panels, in fact, a larger portion of the fiber bundle is affected by complete delamination. By looking at the axial stress distributions (Fig. 20a, c), peak stress values, for the different points B-I, can be noticed in correspondence with the cracks (and with the maximum shear stresses, correspondingly). In the analysis characterized by a light density of the fibers, the complete delamination process is clearly recognizable. For both cases, which are two limit cases concerning the amount of fibers,

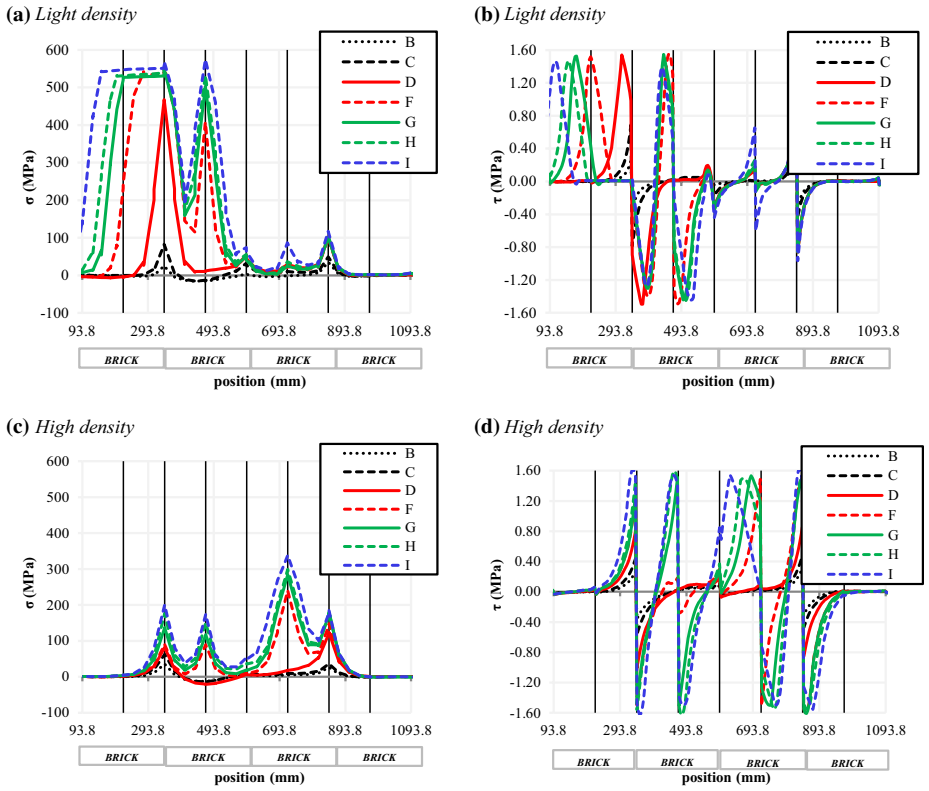

Fig. 20 Axial and shear stress distributions along the fiber 170 for two of the numerical models reported in Table 7: **a**, **b** light density fibers, **c**, **d** high density fibers

it can be noticed that the fiber 170 is subject to a stress much lower than its tensile strength, thus confirming the suitability of the hypothesis of modelling the carbon fibers as a linear elastic material.

In a previous research (Del Zoppo et al. 2019b), a database of diagonal compression tests conducted on masonry panels strengthened with FRCM systems was collected and the effect of different geometrical and mechanical parameters on the shear strength capacity of FRCM strengthened panels was analyzed. With reference to the parametric analyses here conducted, it is worth highlighting that similar findings are achieved, related to the variation of the mortar matrix properties and of the amount of fibers. More in detail, in the cited work (Del Zoppo et al. 2019b), a greater shear capacity of the FRCM strengthened panels was observed by increasing the matrix mechanical ratio, a property depending both on geometrical (i.e. cross section) and mechanical (i.e. compressive or tensile strength) properties of the matrix itself, and by increasing the mechanical ratio of the mesh reinforcement. The role of the matrix mechanical ratio can be here related to the investigated variations in the mortar matrix tensile strength, while the role of the mechanical ratio of the mesh reinforcement corresponds to the considered increase in the amount of fibers. These conclusions, verified over a wide database of experimental tests, support the numerical results here obtained. The variation of other parameters, such as masonry properties, different type of reinforcing fibers, the symmetrical or asymmetrical application of the FRCM systems and the use of mechanical anchorages, analyzed in (Del Zoppo et al. 2019b), have not been discussed in this paper due to the choices about the modelling strategy, but they are surely worth of investigation, especially from the numerical point of view, in future researches.

8 Conclusions

In the present paper, the shear capacity of FRCM strengthened masonry panels subject to diagonal compression tests was numerically investigated. Introducing a *simplified micro-modelling* approach, a novel FE modelling strategy was proposed to simulate the in-plane behavior of FRCM strengthened masonry panels: FRCM reinforcement was discretized by using linear trusses embedded into a cementitious matrix with a proper bond-slip law, calibrated from experimental bond tests (Carozzi et al. 2017). The described modelling approach proved to satisfactorily match the observed experimental behavior both of unreinforced and strengthened masonry panels, subject to diagonal compression tests, and could be also extended to different typologies of FRCM systems, with a proper calibration of the mechanical properties of the materials and of the fiber-mortar matrix bond-slip interface laws.

For the FRCM strengthened panel, the observed force recovery after first cracking was properly described by considering an appropriate bond behavior of the FRCM reinforcement. The comparison between the results from unreinforced and strengthened masonry panels showed an important increment of both the maximum load and maximum displacement capacities, confirming a more ductile behavior of the strengthened panels.

Numerical analyses on the FRCM strengthened panels confirmed that in most of the cases masonry cracked before the external mortar matrix, without introducing a sudden change of slope of the force–displacement curve.

The parametric analyses carried out, considering the variation of some of the main parameters governing the problem, suggested the following considerations:

- Realistic variation of the elastic modulus of the mortar matrix leads to limited variation of the overall shear behavior, if the cracking sequence is not modified (masonry cracks first).
- Mortar matrix tensile strength is important for the definition of the shear capacity of the panel at first cracking; nevertheless, the variation of the mortar matrix tensile strength is correlated with the interface law between mortar matrix and fibers since it determines also a variation in the bond-slip law.
- After the formation of the first crack in the mortar matrix, the shear behavior is governed by the fiber-mortar matrix interface law, especially for what concerns the force drop and the following possible force recovery. High values of interface stiffness and shear strength lead to an effective force recovery.
- The amount of fibers embedded inside the mortar matrix is important after first cracking, unless a really large quantity is considered. It governs the intensity of the force drop and the slope of the following recovery. The second peak is mainly related to the amount of fibers if the masonry panel has the opportunity to properly redistribute the stresses around the main cracks.

Considering the complexity of the problem, where a number of interfaces and fragile behaviors can be found, these first remarks would be further validated trough specific experimental campaigns currently under development. In particular, with the objective of making the introduced FRCM modelling approach more general, different FRCM systems could be modelled and 3D numerical models could be adopted to investigate the shear behavior of multiple-leaves walls or asymmetric reinforcement applications.

Acknowledgements The financial support of the Italian Department of Civil Protection (ReLUIS 2020 Grant—Innovative Materials) is gratefully acknowledged.

Funding Open access funding provided by Alma Mater Studiorum - Università di Bologna within the CRUI-CARE Agreement. The authors have no relevant financial or non-financial interests to disclose.

Declarations

Conflict of interest The authors have no conflicts of interest to declare that are relevant to the content of this article.

References

Aref AJ, Dolatshahi KM (2013) A three-dimensional cyclic meso-scale numerical procedure for simulation of unreinforced masonry structures. Comput Struct 120:9–23. https://doi.org/10.1016/j.compstruc.2013.01.012

Ascione L, Feo L, Fraternali F (2005) Load carrying capacity of 2D FRP/strengthened masonry structures. Compos Part B Eng 36:619–626. https://doi.org/10.1016/j.compositesb.2004.12.004

Ascione L, de Felice G, De Santis S (2015) A qualification method for externally bonded Fibre Reinforced Cementitious Matrix (FRCM) strengthening systems. Compos Part B Eng 78:497–506. https://doi.org/10.1016/j.compositesb.2015.03.079

Atkinson RH, Noland J (1983) A proposed failure theory for brick masonry in compression. In: Proceedings of the 3rd Canadian masonry symposium. Edmonton, Canada, pp 5-1–5-17

Babaeidarabad S, De Caso F, Nanni A (2014) URM walls strengthened with fabric-reinforced cementitious matrix composite subjected to diagonal compression. J Compos Constr 18:04013045. https://doi.org/10.1061/(ASCE)CC.1943-5614.0000441

Balsamo A, Iovinella I, Morandini G (2014) FRG strengthening systems for masonry building. In: NZSEE conference

Balsamo A, Di Ludovico M, Prota A, Manfredi G (2011) Masonry walls strengthened with innovative composites. In: 10th International symposium on fiber-reinforced polymer reinforcement for concrete structures 2011, FRPRCS-10, in conjunction with the ACI Spring 2011 Convention. American Concrete Institute, Vol 2(275), pp 769–786, ACI Special Publication, Tampa, FL, United States

Basili M, Marcari G, Vestroni F (2016) Non-linear analysis of masonry panels strengthened with textile reinforced mortar. Eng Struct 113:245–258. https://doi.org/10.1016/j.engstruct.2015.12.021

Bellini A, Bovo M, Mazzotti C (2019a) Experimental and numerical evaluation of fiber-matrix interface behaviour of different FRCM systems. Compos Part B Eng 161:411–426. https://doi.org/10.1016/j.compositesb.2018.12.115

Bellini A, Shahreza SK, Mazzotti C (2019b) Cyclic bond behavior of FRCM composites applied on masonry substrate. Compos Part B Eng 169:189–199. https://doi.org/10.1016/j.compositesb.2019.04.009

Bertolesi E, Carozzi FG, Milani G, Poggi C (2014) Numerical modeling of Fabric Reinforce Cementitious Matrix composites (FRCM) in tension. Constr Build Mater 70:531–548. https://doi.org/10.1016/j.conbuildmat.2014.08.006

Bertolesi E, Milani G, Poggi C (2016) Simple holonomic homogenization model for the non-linear static analysis of in-plane loaded masonry walls strengthened with FRCM composites. Compos Struct 158:291–307. https://doi.org/10.1016/j.compstruct.2016.09.027

Carozzi FG, Milani G, Poggi C (2014) Mechanical properties and numerical modeling of Fabric Reinforced Cementitious Matrix (FRCM) systems for strengthening of masonry structures. Compos Struct 107:711–725. https://doi.org/10.1016/j.compstruct.2013.08.026

Carozzi FG, Bellini A, D'Antino T et al (2017) Experimental investigation of tensile and bond properties of Carbon-FRCM composites for strengthening masonry elements. Compos Part B Eng 128:100–119. https://doi.org/10.1016/j.compositesb.2017.06.018

Ceroni F, de Felice G, Grande E et al (2014) Analytical and numerical modeling of composite-to-brick bond. Mater Struct 47:1987–2003. https://doi.org/10.1617/s11527-014-0382-8

Comite Euro-International du Beton (1993) CEB-FIB Model Code 1990

Corradi M, Borri A, Castori G, Sisti R (2014) Shear strengthening of wall panels through jacketing with cement mortar reinforced by GFRP grids. Compos Part B Eng 64:33–42. https://doi.org/10.1016/j.compositesb.2014.03.022

de Carvalho Bello CB, Cecchi A, Meroi E, Oliveira DV (2017) Experimental and numerical investigations on the behaviour of masonry walls reinforced with an innovative sisal FRCM system. Key Eng Mater 747:190–195. https://doi.org/10.4028/www.scientific.net/KEM.747.190

de Felice G, Aiello MA, Caggegi C et al (2018) Recommendation of RILEM Technical Committee 250-CSM: test method for Textile Reinforced Mortar to substrate bond characterization. Mater Struct 51:95. https://doi.org/10.1617/s11527-018-1216-x

De Santis S, De Canio G, de Felice G et al (2019) Out-of-plane seismic retrofitting of masonry walls with Textile Reinforced Mortar composites. Bull Earthq Eng 17:6265–6300. https://doi.org/10.1007/s10518-019-00701-5

Del Zoppo M, Di Ludovico M, Balsamo A, Prota A (2019a) Experimental In-Plane Shear Capacity of Clay Brick Masonry Panels Strengthened with FRCM and FRM Composites. J Compos Constr 23:04019038. https://doi.org/10.1061/(ASCE)CC.1943-5614.0000965

Del Zoppo M, Di Ludovico M, Prota A (2019b) Analysis of FRCM and CRM parameters for the in-plane shear strengthening of different URM types. Compos Part B Eng 171:20–33. https://doi.org/10.1016/j.compositesb.2019.04.020

Drucker DC, Gibson RE, Henkel DJ (1957) Soil mechanics and work-hardening theories of plasticity. Trans Am Soc Civ Eng 22:338–346

Faella C, Martinelli E, Nigro E, Paciello S (2010) Shear capacity of masonry walls externally strengthened by a cement-based composite material: an experimental campaign. Constr Build Mater 24:84–93. https://doi.org/10.1016/j.conbuildmat.2009.08.019

Mazzotti C, Ferretti F, Ferracuti B, Incerti A (2016) Diagonal compression tests on masonry panels strengthened by FRP and FRCM. In: Structural analysis of historical constructions: anamnesis, diagnosis, therapy, controls—proceedings of the 10th international conference on structural analysis of historical constructions (SAHC), pp 1069–1076

Ferretti F, Incerti A, Ferracuti B, Mazzotti C (2017) FRCM strengthened masonry panels: the role of mechanical anchorages and symmetric layouts. Key Eng Mater 747:334–341. https://doi.org/10.4028/www.scientific.net/KEM.747.334

Ferretti F, Ferracuti B, Mazzotti C, Savoia M (2019a) Destructive and minor destructive tests on masonry buildings: Experimental results and comparison between shear failure criteria. Constr Build Mater 199:12–29. https://doi.org/10.1016/j.conbuildmat.2018.11.246

Ferretti F, Incerti A, Tilocca AR, Mazzotti C (2019b) In-plane shear behavior of stone masonry panels strengthened through grout injection and fiber reinforced cementitious matrices. Int J Archit Herit. https://doi.org/10.1080/15583058.2019.1675803

Gabor A, Ferrier E, Jacquelin E, Hamelin P (2005) Analysis of the in-plane shear behaviour of FRP reinforced hollow brick masonry walls. Struct Eng Mech 19:237–260. https://doi.org/10.12989/sem.2005.19.3.237

Gabor A, Bennani A, Jacquelin E, Lebon F (2006) Modelling approaches of the in-plane shear behaviour of unreinforced and FRP strengthened masonry panels. Compos Struct 74:277–288. https://doi.org/10.1016/j.compstruct.2005.04.012

Garofano A, Ceroni F, Pecce M (2016) Modelling of the in-plane behaviour of masonry walls strengthened with polymeric grids embedded in cementitious mortar layers. Compos Part B Eng 85:243–258. https://doi.org/10.1016/j.compositesb.2015.09.005

Gattesco N, Boem I (2015) Experimental and analytical study to evaluate the effectiveness of an in-plane reinforcement for masonry walls using GFRP meshes. Constr Build Mater 88:94–104. https://doi.org/10.1016/j.conbuildmat.2015.04.014

Gattesco N, Boem I, Dudine A (2015) Diagonal compression tests on masonry walls strengthened with a GFRP mesh reinforced mortar coating. Bull Earthq Eng 13:1703–1726. https://doi.org/10.1007/s10518-014-9684-z

Giamundo V, Sarhosis V, Lignola GP et al (2014) Evaluation of different computational modelling strategies for the analysis of low strength masonry structures. Eng Struct 73:160–169. https://doi.org/10.1016/j.engstruct.2014.05.007

Giaretton M, Dizhur D, Garbin E et al (2018) In-plane strengthening of clay brick and block masonry walls using textile-reinforced mortar. J Compos Constr 22:04018028. https://doi.org/10.1061/(ASCE)CC.1943-5614.0000866

Grande E, Milani G (2018) Interface modeling approach for the study of the bond behavior of FRCM strengthening systems. Compos Part B Eng 141:221–233. https://doi.org/10.1016/j.compositesb.2017.12.052

Grande E, Milani G, Sacco E (2008) Modelling and analysis of FRP-strengthened masonry panels. Eng Struct 30:1842–1860. https://doi.org/10.1016/j.engstruct.2007.12.007

Incerti A, Ferretti F, Mazzotti C (2019a) FRCM strengthening systems efficiency on the shear behavior of pre-damaged masonry panels: an experimental study. J Build Pathol Rehabil 4:14. https://doi.org/10.1007/s41024-019-0053-9

Incerti A, Tilocca AR, Ferretti F, Mazzotti C (2019b) Influence of masonry texture on the shear strength of FRCM reinforced panels. In: RILEM bookseries, pp 1623–1631

Incerti A, Vasiliu A, Ferracuti B, Mazzotti C (2015) Uni-axial compressive tests on masonry columns confined by FRP and FRCM. In: 12th International symposium on fiber reinforced polymers for reinforced concrete structures (FRPRCS-12) & 5th Asia-Pacific conference on fiber reinforced polymers in structures (APFIS-2015) joint conference

Leone M, Aiello MA, Balsamo A et al (2017) Glass fabric reinforced cementitious matrix: tensile properties and bond performance on masonry substrate. Compos Part B Eng 127:196–214. https://doi.org/10.1016/j.compositesb.2017.06.028

Lignola GP, Caggegi C, Ceroni F et al (2017) Performance assessment of basalt FRCM for retrofit applications on masonry. Compos Part B Eng 128:1–18. https://doi.org/10.1016/j.compositesb.2017.05.003

Lourenço PB (1996) Computational strategies for masonry structures. Delft University of Technology

Lourenço PB, Rots JG (1997) Multisurface interface model for analysis of masonry structures. J Eng Mech 123:660–668. https://doi.org/10.1061/(ASCE)0733-9399(1997)123:7(660)

Macorini L, Izzuddin BA (2011) A non-linear interface element for 3D mesoscale analysis of brick-masonry structures. Int J Numer Methods Eng 85:1584–1608. https://doi.org/10.1002/nme.3046

Masia MJ, Han Y, Correa MRS (2006) Torsion testing for the characterisation of the shear behaviour of mortar joints in masonry. Mason Int Br Mason Soc 19:77–88

Mazzotti C, Murgo FS (2015) Numerical and experimental study of GFRP-masonry interface behavior: Bond evolution and role of the mortar layers. Compos Part B Eng 75:212–225. https://doi.org/10.1016/j.compositesb.2015.01.034

Menna C, Asprone D, Durante M et al (2015) Structural behaviour of masonry panels strengthened with an innovative hemp fibre composite grid. Constr Build Mater 100:111–121. https://doi.org/10.1016/j.conbuildmat.2015.09.051

Mininno G, Ghiassi B, Oliveira DV (2017) Modelling of the in-plane and out-of-plane performance of TRM-strengthened masonry walls. Key Eng Mater 747:60–68. https://doi.org/10.4028/www.scientific.net/KEM.747.60

Murgo FS, Mazzotti C (2017) Numerical analysis of masonry confined by FRCM. Key Eng Mater 747:558–566. https://doi.org/10.4028/www.scientific.net/KEM.747.558

Murgo FS, Mazzotti C (2019) Masonry columns strengthened with FRCM system: Numerical and experimental evaluation. Constr Build Mater 202:208–222. https://doi.org/10.1016/j.conbuildmat.2018.12.211

Mustafaraj E, Yardim Y (2016) Usage of ferrocement jacketing for strengthening of damaged unreinforced masonry (URM) walls. In: 3rd International Balkans conference on challenges of civil engineering, 3-BCCCE

Nerilli F, Ferracuti B (2018) Investigation on the FRCM-masonry bond behaviour. In: CICE 2018—9th international conference on fibre-reinforced polymer (FRP) composites in civil engineering. Paris, France

Parisi F, Iovinella I, Balsamo A et al (2013) In-plane behaviour of tuff masonry strengthened with inorganic matrix–grid composites. Compos Part B Eng 45:1657–1666. https://doi.org/10.1016/j.compositesb.2012.09.068

Penna A (2015) Seismic assessment of existing and strengthened stone-masonry buildings: critical issues and possible strategies. Bull Earthq Eng 13:1051–1071. https://doi.org/10.1007/s10518-014-9659-0

Penna A, Morandi P, Rota M et al (2014) Performance of masonry buildings during the Emilia 2012 earthquake. Bull Earthq Eng 12:2255–2273. https://doi.org/10.1007/s10518-013-9496-6

Petersen RB (2009) In plane shear behavior of unreinforced masonry panels strengthened with fiber reinforced polymer strips, University of Newcastle, Australia

Petersen RB, Masia MJ, Seracino R (2010) In-plane shear behavior of masonry panels strengthened with NSM CFRP strips. II: finite-element model. J Compos Constr 14:764–774. https://doi.org/10.1061/(ASCE)CC.1943-5614.0000137

Petersen RB, Ismail N, Masia MJ, Ingham JM (2012) Finite element modelling of unreinforced masonry shear wallettes strengthened using twisted steel bars. Constr Build Mater 33:14–24. https://doi.org/10.1016/j.conbuildmat.2012.01.016

Van der Pluijm (1999) Out-of-plane bending of masonry behaviour and strength,Technische Universiteit Eindhoven

Prota A, Marcari G, Fabbrocino G et al (2006) Experimental in-plane behavior of tuff masonry strengthened with cementitious matrix-grid composites. J Compos Constr 10:223–233. https://doi.org/10.1061/(ASCE)1090-0268(2006)10:3(223)

Rots JG (1997) Structural masonry: an experimental/numerical basis for practical design rules. Balkema, Rotterdam

Sarhosis V, Lemos JV (2018) Detailed micro-modelling of masonry using the discrete element method. Comput Struct 206:66–81

Schellekens JCJ (1992) Computational strategies for composite structures Delft Unversity of Technology

Türkmen ÖS, De Vries BT, Wijte SNM, Vermeltfoort AT (2020) In-plane behaviour of clay brick masonry wallettes retrofitted with single-sided fabric-reinforced cementitious matrix and deep mounted carbon fibre strips. Bull Earthq Eng 18:725–765. https://doi.org/10.1007/s10518-019-00596-2

Van der Pluijm R (1997) Non-linear behavior of masonry under tension. Heron 42:25–54

van Zijl GPA (2004) Modeling masonry shear-compression: role of dilatancy highlighted. J Eng Mech 130:1289–1296. https://doi.org/10.1061/(ASCE)0733-9399(2004)130:11(1289)

van Zijl GPAG, de Vries PA (2005) Masonry wall crack control with carbon fiber reinforced polymer. J Compos Constr 9:84–89. https://doi.org/10.1061/(ASCE)1090-0268(2005)9:1(84)

Verhoef LGW, van Zijl GPA (2002) Re-strengthening of brickwork to reduce crack width. Adv Eng Softw 33:49–57. https://doi.org/10.1016/S0965-9978(01)00051-5

Wang C, Forth JP, Nikitas N, Sarhosis V (2016) Retrofitting of masonry walls by using a mortar joint technique; experiments and numerical validation. Eng Struct 117:58–70. https://doi.org/10.1016/j.engstruct.2016.03.001

Wang X, Ghiassi B, Oliveira DV, Lam CC (2017) Modelling the non-linear behaviour of masonry walls strengthened with textile reinforced mortars. Eng Struct 134:11–24. https://doi.org/10.1016/j.engstruct.2016.12.029

Yardim Y, Lalaj O (2016) Shear strengthening of unreinforced masonry wall with different fiber reinforced mortar jacketing. Constr Build Mater 102:149–154. https://doi.org/10.1016/j.conbuildmat.2015.10.095